Ocean Sci. Discuss., 6, 3057–3100, 2009
www.ocean-sci-discuss.net/6/3057/2009/

Ocean Science Discussions

This discussion paper is/has been under review for the journal Ocean Science (OS).
Please refer to the corresponding final paper in OS if available.

Numerical simulations of spreading of the Persian Gulf outflow into the Oman Sea

M. Ezam[1], **A. A. Bidokhti**[1,2], **and A. H. Javid**[1]

[1]Faculty of Marine Science and Technology, Science and Research Branch,
Islamic Azad University, P. O. Box 14155-775, Tehran, Iran
[2]Institute of Geophysics, University of Tehran, P. O. Box 14155-6466, Tehran, Iran

Received: 1 December 2009 – Accepted: 3 December 2009 – Published: 14 December 2009

Correspondence to: M. Ezam (ezam@srbiau.ac.ir)

Published by Copernicus Publications on behalf of the European Geosciences Union.

Abstract

A three dimensional numerical model namely, (Princeton Ocean Model) and some observational data are used to study the Persian Gulf outflow structure and its spreading pathways during two different time of the year, mid-winter and early summer. A few available observations show that the Persian Gulf outflow source water exhibits seasonal variations in temperature and salinity. The numerical model is set up by CTD measurements at its western boundary and monthly surface wind speed on the model domain from ICAODS data. The results show that the outflow originates from two branches at different depths in the Persian Gulf. The permanent branch that may exist during the whole year in deeper parts at about 40 m and originates from inner parts of the Persian Gulf and the other one is a seasonal branch that starts to form the vicinity of southern coast during winter months (February). Near the Strait of Hormuz the two branches are jointed together and form the main outflow source. Our findings reveal that during the winter the outflow boundary current detaches from the coast just at the Ras Al Hamra Cape, however for the summer the outflow seems to follow the coast even after this Cape, and appears to separate from the coast at the Ras Al Hadd Cape. This behavior is explained as follow: more saline outflow during February causes higher density and so sinking to deeper zone during the winter. Thus, it moves to deeper parts at about 500 m in contrast with that of May which is at about 300 m. During February at Ras Al Hamra Cape the deeper and stronger outflow is more affected by the steep topography slope leading to vortex stretching mechanism which causes it to meander as an "*S*" shape, while during May, weaker and shallower outflow is less influenced by bottom topography and so it continues along the boundary.

1 Introduction

The Persian Gulf is a semi-enclosed marginal sea located between 22–30 latitudes and extending in northwest-southeast direction and is connected to the Indian ocean

OSD

6, 3057–3100, 2009

through the Strait of Hormuz and the Oman Sea. High evaporation rate between 1.5–2 m yr^{-1} (Chao et al., 1992) and the shallowness of the Persian Gulf especially in vicinity of southern coasts leads to formation of saline and dense water with maximum salinities up to about 57 in shallow estuaries along the southern coasts (John et al., 1990), although the maximum salinity range over most of the Persian Gulf is about 40.0–40.5 (Brewer et al., 1978; Chao et al., 1992). Most saline water in the Persian Gulf is observed during the first half of year compared to second half (Bower et al., 2000; Johns, 2003), and it is cooler by several degrees during February–June compared to July–January. The saline water sinks to the deeper zone due to higher density and form a density front. The dense water exits the Persian Gulf through the Strait of Hormuz as a bottom boundary current, banked against southern coasts, and fresher Indian Ocean water enters the Persian Gulf as a surface current mostly on the northern side (Brewer el al., 1978; Chao et al., 1992; Swift and Bower, 2003). Dynamics of dense fluids descending on an inclined boundary have been the subject of some studies in oceanography.

Jungclaus and Mellor (2000) investigated the Mediterranean outflow through the Strait of Gibraltar using a three-dimensional numerical model (POM). They concluded that the outflow is controlled by the pressure gradient and Coriolis force, entrainment and bottom friction. They speculated that the combined effects of the stratification, differential entrainment, and routing by topography lead to evolution of a two core structure in the bottom layer. After the outflow passes the Cape St. Vincent it become hydro-dynamically unstable and lenses of saline water shed from the core and carry the outflow characteristics into the Atlantic Ocean.

Pous et al. (2004) revealed shot-term variability of the outflow (about two weeks) by direct measurements using sur-drift buoys, hydrological and ADCP data. They attributed this variability to different mechanisms such as advections of the outflow, meander growth and eddy detachment from the outflow as it spreads into the Oman Sea, and diffusion of thermohaline properties of the outflow into the adjacent water masses. Some ADCP measurements in the Strait of Hormuz by Johns (2003) indi-

OSD
6, 3057–3100, 2009

cated no strong variability in outflow transport with the mean annual value of about the 0.2–0.25 Sv.

Matsuyama et al. (1998) investigated the vertical structure of the current and its time variations using ADCP measurement during December 1993–January 1994 in the Strait of Hormuz. They argued that the effective water exchange in the Strait occurs during the neap tide, while the density front (outflow) exists during spring tide as well. Density front formation depends on the strength of density stratification under the same tidal current, because the vertical mixing due to tidal current is suppressed by the strong density stratification.

Bidokhti and Ezam (2009) considered the vertical structures of the outflow and surrounding waters in the Oman Sea using ROMPE expedition of 1992 measurements (Reynolds, 1993). They argued that the outflow in the Oman Sea exhibits layering structures and attributed them to double diffusive convection as well as internal wave activities. They also used a simple dynamics model based on conservation of potential vorticity and assumption of geostrophic adjustment to estimate the outflow average velocity and width as well as testing some scenarios about salinity change and its effect on the outflow velocity and width without entrainment effects.

In this paper, in order to reveal outflow T-S characteristics in the Strait of Hormuz and Oman Sea (for comparison with the numerical results), we first present some CTD measurements from ROMPE expedition in 1992 during January–February 1992 (leg 6) and May–June 1992 (leg 1). This has also been considered in some detail in Bidokhti and Ezam (2009). Second (and mainly), we use a three-dimensional numerical model (Princeton Ocean Model) to study the spreading pathways of the residual currents in the model domain including some of the large scale features in Gulf of Oman. The currents induced by only wind forcing at the surface, and the currents induced by simultaneous forcings of wind, and buoyancy at the western boundary of the model domain, are considered. The simulations are performed at two different times of the year (mid winter and early summer), when the CTD measurements are available and are utilized to bring about buoyancy forcing at the western boundary of the model domain. In ad-

OSD
6, 3057–3100, 2009

dition, surface wind fields are prepared from averaged monthly wind over the model domain.

We also do not include tidal effects in our simulations, as we assume that the condition of the outflow is during the neap tide (as mentioned by Matsuyama et al. (1998), during the neap tide, tidal front disappears and outflow is at its maximum discharge). The outflow pathways, descending and mixing with surrounding waters, and eddy generation mechanisms in the Oman Sea are also investigated.

2 The approach

2.1 Observational data

Hydrographic measurements that are used here are those of the ROPME expedition in 1992. Locations of CTD measurement stations during January–February (leg 1) and May–June (leg 6) are shown in Fig. 1. The CTD Measurements collected in this expedition are the only comprehensive ones and therefore are appropriate for this study. In addition, data were collected at two different times of the year and so the temporal variability of the outflow can be considered to some extent. Here we are not going to consider the data again. A good review about the ROPME 1992 expedition and the data can be found in Reynolds (1993).

2.2 Numerical model

The Princeton Ocean Model (POM, e.g. Mellor, 2003) is based on hydrostatic primitive equations with Boussinesq approximation, terrain following vertical coordinate (sigma coordinate) system in the vertical and general orthogonal curvilinear system in the horizontal. The numerical grid employed for the spatial discretization is C-grid as presented by Arakawa and Mesinger (1976). The model uses the mode splitting technique which is the separation of fast moving surface gravity waves in 2-D barotropic mode and solving them using high order explicit finite difference methods with external time step, from

OSD
6, 3057–3100, 2009

the slower moving one in 3-D baroclinic mode and solving them implicitly with internal time step. In the numerical solution the external and internal time steps are determined from stability condition (CFL as presented by Courant-Friedrichs-Levy). For the external mode (barotropic mode), in the transport equations, constrain of the time step is set to:

$$\Delta t_{\mathrm{E}} \leq \frac{1}{C_t}\left|\frac{1}{\delta x^2}+\frac{1}{\delta y^2}\right|^{-1/2} \tag{1}$$

where $C_{\mathrm{t}} = 2(gH)^{1/2} + U_{\mathrm{max}}$; U_{max} is the maximum expected velocity in the domain (here $1\,\mathrm{ms}^{-1}$), and Δx and Δy are horizontal grid spacing which are about 3.5 km in this modeling.

For typical coastal ocean condition, the ratio of internal to external time step is of order of 30–80 (Ezer et al., 2002). So we assume it to be equal to 80.

The vertical mixing coefficients in the model are calculated by a second order turbulence closure model, namely Mellor-Yamada level 2.5 model of turbulence that is characterized by two quantities, turbulence kinetic energy and turbulent length scale. The background vertical mixing coefficients for temperature, salinity and momentum were set to $2\times10^{-5}\,\mathrm{m}^2\,\mathrm{s}^{-1}$ as a default in POM. However, various studies have shown the sensitivity of the model results to different background vertical mixing coefficient. For example, Berdeal et al. (2002) investigated the plume structure from Colombia River on the US west coasts and showed that when this background value increases to $10^{-4}\,\mathrm{m}^2\,\mathrm{s}^{-1}$ and especially to $10^{-3}\,\mathrm{m}^2\,\mathrm{s}^{-1}$ the plume special structure changes dramatically. In addition, the effects of increasing the vertical mixing coefficient are especially noticeable in the up-shelf penetration of the plume and extension of its bulge. They also showed that if the background vertical diffusivity increases to $10^{-4}\,\mathrm{m}^2\,\mathrm{s}^{-1}$ more upstream intrusion is noticeable. Garvine (1999) suggested for high Richardson number, the vertical mixing coefficients revert to background value set by the user and in this case, holding the constant vertical mixing coefficients at a constant value of $10^{-4}\,\mathrm{m}^2\,\mathrm{s}^{-1}$ and $10^{-3}\,\mathrm{m}^2\,\mathrm{s}^{-1}$ instead of using the closure scheme yields almost the

OSD
6, 3057–3100, 2009

identical results.

Horizontal diffusions in the model are calculated from Smogorinsky diffusivity formula as:

$$A_M = C\,\Delta x\,\Delta y\,\frac{1}{2}\left[\left(\frac{\partial u}{\partial x}\right)^2 + \left(\frac{\partial v}{\partial y}\right)^2 + \left(\frac{\partial w}{\partial z}\right)^2\right]^{1/2} \quad (2)$$

where u, v and w are velocity components in horizontal and vertical respectively, and C is a non-dimensional HORCON parameter and has been recommended to be in range between 0.1–0.2 (Mellor, 2003), (here it is chosen to be 0.2).

2.3 The model domain and data

The model domain is located in 21.5–27.4° N and 54–61° E that includes the eastern part of the Persian Gulf, the Oman Sea and north-west of the Indian Ocean as indicated in Fig. 2. The bathymetry of the region were extracted from ETOP02, which contains global earth topography including land with 2 min (roughly 4 km) resolution, and were interpolated to the grid size of model. The horizontal grid resolutions are approximately 3.5 km and we employed 32 vertical layers with logarithmic distribution in order to better represent the surface and bottom boundary layers.

2.4 Initial and boundary conditions

Initial temperature and salinity of the model domain were extracted from WOA05, which contains global monthly and annual temperature and salinity with one and one forth degree resolutions. The initial temperature and salinity were prepared from climatological annual mean and interpolated on model grid in horizontal and vertical. The wind stress is assumed as the only forcing on the surface of the model domain and is acquired from ICOADS mean monthly wind which includes global wind data with one degree resolution. Figure 3 shows the wind fields on the model domain for February and May 1992 after processing and interpolation.

OSD

6, 3057–3100, 2009

The wind dependent drag coefficient (Geernaert et al., 1986), for calculating the wind stress on the surface, was assumed to be:

$$C_{\mathrm{D}}^{\mathrm{S}} = 10^{-3}\left(0.43 + 0.097|U_{10}|\right) \tag{3}$$

where, $|U_{10}|$ is the magnitude of wind speed at 10 m above the sea level.

For the external mode velocities at open boundaries, a type of radiation boundary condition (e.g. Mellor, 2004) of the following form were employed (right hand side of Eq. (4) may not be zero when tide or barotropic velocities are assumed):

$$H\overline{U} \pm c_e \eta = 0 \tag{4}$$

where H, is the water depth at corresponding grid, $\overline{U}$ is the external mode velocity, c_e is the external mode phase speed and is equal to $\sqrt{gH}$ and η is the sea surface elevation at corresponding grid.

For the internal mode velocity, Sommerfeld radiation condition of the form:

$$\frac{\partial u}{\partial t} + c_i \frac{\partial u}{\partial n} = 0 \tag{5}$$

is used. Where n is a direction perpendicular to the open boundary and c_i is the phase speed of internal mode propagation and is calculated using Orlanski scheme (1976).

The open boundary conditions for temperature and salinity were set up by the CTD measurements (ROPME 1992) at the western boundary. According to the survey of CTD measurements, western boundary of the model was selected as the region that the outflow has descended on the bottom and the thermohaline characteristics are indicative of the density front (outflow) tending to move eastward towards the Strait of Hormuz. Hence, we use the CTD data along the western boundary for buoyancy forcing (thermohaline forcing). For this aim, CTD measurements of the two legs of ROPME expedition (1992), one during January–February and other one during May–June were assumed as thermohaline characteristics during simulation times. It is necessary to say that the number of measurement stations along the boundary were limited, especially in the southern part. However, the data was interpolated on the model grid at the

OSD
6, 3057–3100, 2009

western boundary in horizontal and vertical (sigma levels). Figure 4 exhibits the temperature and salinity transects for February and May on the western boundary after processing the CTD data.

For the temperature and salinity on the eastern and southern open boundaries, while there are inflow to the domain, due to the lack of direct measurements, mean monthly temperature and salinity for February and May from WOA05 with one forth degree resolution were utilized and interpolated on model gird in horizontal and vertical, however, for the outflow an upstream advection boundary condition was used (e.g. Kantha and Klayson, 2000; Mellor, 2003).

3 Results and discussion

3.1 Wind driven currents

Initially, in order to consider the patterns of wind driven current, the model was run with only mean monthly wind at the sea surface. Figure 5 shows the mean wind driven currents on the model domain at depth −1 m in February and May. It could be deduced from the figure that in February the eastward surface currents regime in the Strait of Hormuz is intensified while in May this regime is being weakened, however, at this time nearly strong eastward current is observed along Iranian coasts that turns right due to the Ekman drift in the south of the Qeshm Island and is disappeared before reaching the Strait of Hormuz. The weaker eastward currents in the Strait during May, could allow surface Indian Ocean waters to penetrate more into the Persian Gulf and thus, water exchange between Persian Gulf and Gulf of Oman can be intensified during this time.

In February, in the Oman Sea, a relatively intense eastward current is observed along the Iranian coast between 57–60° E which may lead to strong upwelling in this region in February. Another discernible current in this time is a north-westward current in the Oman Sea between 56.5–58° E and 23–25.5° N that turns right (due to bottom

OSD
6, 3057–3100, 2009

topography and Coriolis effects) and join the eastward current at 57° E. In May, in contrast to that of February, in the Oman Sea a cyclonic circulation between 59.5–61° E and 22.5–24° N is beginning to form that is the result of commencing South western Monsoon in this region.

3.2 The flow cross-sections

In the prior section, pattern of wind driven currents in response to only wind forcing was considered. Here, the results of the model simulations with both buoyancy force on the western boundary and mean monthly wind stresses at the surface are considered. The results of the simulations show that according to the transects of temperature and salinity in the Persian Gulf (transect CD, Fig. 6) in February at depth 0–40 m, the temperature in southern part is lower than that in northern part which may be due to higher evaporations caused by stronger effects of cold surface winds blowing in the region during winter months and also smaller water depths, while in May this regime is reversed because of beginning of summer heating and weakening of north westerly cold surface winds. The salinity transect in February shows the formation of saline water in Southern part of the path CD with highest salinities at depths of 10–40 m with values more than 41 psu, while it disappears in May. In the regions deeper that 40 m depths masses of saline water are observed in both months with a little higher salinities in February.

As a whole, combinations of higher salinity and lower temperature in February cause formation of high dense waters with densities more that 1030 kgm^{-3} in the southern part, especially at depths between 10 to 40 m. Hence, it appears that the Persian Gulf outflow originates from two branches. One permanent branch that exists permanently during the whole of the year in deeper than 40 m and may be started to form from inner parts of the Persian Gulf, and one seasonal branch which begins to form in the winter months and originates from shallow southern parts. The seasonal branch after formation, because of its higher density relative to surrounding water, while moving eastward due to buoyancy, sinks to the deeper zone and joints the permanent branch.

Finally these two branches form the Persian Gulf outflow in the bottom of the Gulf in the east of the Strait of Hormuz (transect IJ).

Figures 7 and 8, show transects of temperature, salinity, sigma-*T* and velocity components along path IJ for February and May. In February, temperature transects show low vertical temperature differences (about 3 °C), while in May the seasonal thermocline begins to form and vertical temperature differences up to 8 °C are observed. The outflow temperature in deeper than 60 m zones is nearly the same in some locations and is about 21 °C, in other parts of the outflow the temperature is slightly higher in May due to mixing with warmer surrounding water in comparison with February (22.5 °C versus 21 °C).

For both months near the surface, a water mass with a higher temperature relative to surroundings are observed in the eastern part of the transects which is an evidence of a permanent anti-cyclonic eddy and is clear in velocity transects in Fig. 8 and also in horizontal sections of temperature filed (Fig. 10). During May at the center of transect, an increase of temperature at depths 40–50 m is observed which is a sign of a cyclonic eddy and is also evident in velocity transects.

The salinity transects along IJ path show thicker and higher saline water near the bottom in February relative to May (more than 40 psu versus 39 psu). In the eastern half of these transects, salinities are nearly the same from surface down to the depth of 60 m for both months and are about 36.5 psu. In the western half of the path, salinities are higher in May especially above the depth of 30 m. It may be resulted from the advection of saline water by eddies in the region and also higher mixing and entrainment with surrounding waters during May because of lower density stratification.

As are observed in sigma-*T* transects in IJ path, during February (winter months) a two layer density regime is observed, an upper layer with sigma-*T* of about 25.5 kgm^{-3}, and lower layer with sigma-*T* values more than 29 kgm^{-3}.

In these transects pycnostads (characteristic of strong baroclinic ocean currents) are observed showing layer with almost constant density. During May (summer months) three layer stratification is observed, an upper low density layer with sigma-*T* values

OSD
6, 3057–3100, 2009

of about 23 kgm^{-3}, the intermediate layer with a value of about 25.5 kgm^{-3} and lower layer with a value of about 27.5 kgm^{-3}. It can be concluded from these values that during February higher density differences between benthic layer and upper layer (about 3 kgm^{-3}) leads to higher stratification and therefore the entrainment and mixing between the outflow and upper layer decreases in comparison with May in which the density difference is weaker in water column (about 2 kgm^{-3}).

The velocity transects along IJ path (Fig. 8), exhibits the highest velocities in depths of 50–70 m where the effects of bottom friction are least. The direction of the outflow at these depths is mainly southward. The westward component of the flow may be induced by stronger Coriolis force due to higher velocity which causes the flow to turn right in north hemisphere. In the bottom boundary layer, the direction of the outflow is still southward which is due to stronger bottom friction (Ekman effect).

The T and S characteristics of the outflow along transect MN are shown in Fig. 9. The main outflow branch is identified in salinity and temperature transects, as saltier and warmer water mass relative to surrounding water is banked against western coast. In addition, some patches with higher salinity and warmer water are also observed at the same depth of the outflow that can be as the result of instability of the outflow plume (see the next section). The outflow at transect MN is warmer and less salty during May that is due to warmer and fresher source water characteristics (Persian Gulf water) at this time. In February, due to saltier and colder source water, and also lesser entrainment and mixing in comparison with May, the outflow appears saltier and colder. These lead to formation of denser outflow during February and thus intruding into the deeper zone to reach the equilibrium depth. Thus, the equilibrated outflow is observed with mean depths of 300 m and 500 m during May and February respectively. The sigma-T transects also confirm that the outflow has reached its equilibrium level, since after reaching this depth, nearly no horizontal density differences are observed at the depth of the outflow between source water and the surrounding waters.

OSD
6, 3057–3100, 2009

3.3 Horizontal fields

The horizontal sections of temperature and salinity with overlaid velocity field at depth 1m are shown in Fig. 10 for February and May. From the figure we could conclude that the saltier Persian Gulf water during February especially in the southern part, the intrusion of this water mass into the Oman Sea are lower than that of May in which the water is warmer and less salty. This is probably because of higher source water density during February that causes it to sink more into the deeper layers while it is flowing eastward to exit the Gulf and so it disappears from the surface inside the Gulf. In addition, during May, pattern of wind driven eastward currents which are more effective in the inner Gulf may contribute the more spreading of the Persian Gulf water into the Oman Sea at the upper layers. As a whole, it could be concluded that during May because of weaker eastward wind driven currents in the Strait of Hormuz, more spreading of Oman sea surface water into the Persian Gulf occurs as a current in vicinity of Iranian coasts, and therefore stronger water exchange occurs during May in contrast with that of February.

A warm center anti-cyclonic eddy is observed during both months in the south east of the Strait of Hormuz that may have been generated by interaction between the Persian Gulf and the Oman sea waters as a result of instability. In addition, pattern of the wind driven current during Feburary (Fig. 5) could be the reason for intensifying this eddy during this time. During February in the Oman Sea the only major circulation is an anti-cyclonic motion between 58.5–60° E and 23.5–25° N with mean velocities of order of 0.5 ms^{-1}. This eddy has been observed by previous works (e.g. Senju et al., 1998). For comparison the geostrophic velocities at 17 February 1993 from NOAA/PMEL has also been shown in Fig. 11.

In May, the commencing of the south westerly Monsoon influences the circulation pattern in the Oman Sea and three major circulations are formed during this time (Fig. 10). One is a cyclonic cold center circulation formed between 59–60.5° E and 22.5–24° N with mean velocity of order of 0.8 ms^{-1}. The second circulation is an anti-

OSD
6, 3057–3100, 2009

cyclonic eddy with a relatively warm center between 58–59° E and 24.5–25.2° N with mean velocity of about 0.2 ms^{-1}. Our findings indicate that these eddies are probably unstable so that after the numerical solution reaches a quasi steady state they begin to oscillate as dipole with time scale of about 100 days. Namely, during this period the anti-cyclonic eddy is getting attenuated while the cyclonic one is getting intensified. Then, again the anticyclone begins to grow and this cycle is repeated. For baroclinic vortices produced by a constant flux of buoyant fluid from a point source, Griffiths and Linden (1981) using a two layer model, showed that a vortex grows in radius and depth until the parameter $\theta\gamma^{-1/2}$ decreases beyond a critical value (about 0.02). Where γ is defined as the depth ratio of h_1/h_2 (h_1 and h_2 are depths of the layers), $\theta = g' h_1/f^2R^2$, where R is the vortex radius, f and g' are the Coriolis parameter and the reduced gravity respectively. At this point the vortex becomes unstable to non-axisymmetric distributions with azimuthal wave number $n = 2$.

The Rossby number for the cyclonic cold center eddy (that mentioned above) is about 0.2. Thus, if we properly assume it as a borolinic generated vortex, with applying the above reasoning with $g' = 0.004\,ms^{-2}$, $h_1 = 600$ m, $h_2 = 2400$ m, $f = 5.9 \times 10^{-5}\,s^{-1}$ and $\theta = 0.02$ the maximum radius that the eddy could grow before it begins to be unstable, is about 60 km. This radius is nearly consistent with that we observe for the cyclone (about 70 km) before it begins to go unstable and the anti-cyclone eddy in the north-west of the eddy forms.

The circulation pattern in May (Fig. 10) is in good agreement with the finding of Paus, et al. (2004) that is based on filed observations during October and early November 1999 which is shown in Fig. 11. However, the locations of eddies in the simulation results are somewhat not the same as that shown by the observations of Paus, et al. (2004). This may be due to the differences in the time of their measurement with that of this study.

Elliott and Savidge (1990) by analyzing hydrographic and ADCP data, that were collected in the coastal water of Oman during summer Monsoon, found a strong surface temperature gradient near the Ras al Hadd (located at approximately 22.3° N and

OSD
6, 3057–3100, 2009

59.7° E) and a geostrophic surface flow with velocities exceeding 1 ms^{-1}. In addition, they showed that when the flow reaches the Ras Al Hadd, it turns offshore towards the northeast and forms the Ras Al Hadd Jet (front). Tang et al. (2002) with processing OCTS (Ocean Color and Temperature Scanner), Sea-view Wide Field of view Sensor (SeaWiFS) and AVHRR sea surface temperature images of northern Arabian Sea in November 1996, have also specified the phytoplankton blooms associated a clod center eddy in the Gulf of Oman. They showed that the bloom had a round shape with 100 km diameter and appeared as a cyclonic eddy feature between 60.5° E– 24° N. In addition, the eddy accompanied with an anti-cyclonic eddy at its southwest with lower chlorophyll values located at 61.5° E– 22.5° N.

As a whole, the overall features of formation of Ras Al Hadd front and the cylonic eddy are consistent with our simulation for May. But, it is necessary to say that the study of circulation patterns in the Oman Sea can be performed as another study with more attention to eddy generation mechanisms and their dependence on short time varying surface forcing and outflow as well. Here we mainly intended to study the Persian Gulf outflow spreading pathways and its role on the formations of eddies in the Oman Sea and attempt to minimize the open boundary effects by choosing them as far as possible.

The extended view of the outflow properties including temperature, salinity and velocity filed at the Strait of Hormuz at depth 80 m are shown in Fig. 12. The figure shows the outflow source water has nearly equal temperature especially at the Strait of Hormuz for both months, but the source water salinity is higher by more than 1 psu during February. These lead to denser outflow during February relative to that of May (29 kgm^{-3} versus 28 kgm^{-3}) and higher outflow maximum velocities during February (0.74 ms^{-1} versus 0.66 ms^{-1}). These results are nearly consistent with some other previous works. Bidokhti and Ezam (2009) estimated the average values for outflow velocity using a simple dynamical model as 0.53 ms^{-1} (winter) and 0.42 ms^{-1} (summer). Bower et al. (2000), using a single layer outflow model recommended that the outflow reaches its maximum speed of 0.55 ms^{-1} (winter) and 0.4 ms^{-1} (summer) and

OSD
6, 3057–3100, 2009

attributed these maximums to the continental shelf effects where the bottom slope suddenly increases and causes the outflow to gain more acceleration. However, the source water outflow characteristics in Bower model are slightly different with those of this study.

In contract to May, in February at 25° N the outflow nearly disappears that is because of its higher density that causes its main part to sink to deeper zone. Also, some eddies with mean diameter of about 50 km and velocities of about 0.15 ms^{-1} are observed near the interface of the outflow with ambient water during February.

Figures 13 and 14 show the horizontal fields of the salinity and temperature and their corresponding velocities at depths 300 m and 500 m, respectively. It can be deduced from the figures that the outflow during May mainly appears in the shallower zone relative to that of February because of its lower density. So during May, the outflow that is more evident at the depth of 300 m continues its propagation as a narrow boundary current in vicinity of southern and western coasts. After passing the Ras Al Hamra Cape (located at 58.5° E and 23.5° N) the outflow widens in width as observed by Paus et al. (2004), while it loses its heat and salinity owing to mixing with ambient water. When it reaches the Ras Al Hadd region (located at 59.7° E and 25.5° N) it turns to offshore (east) and acquires a cyclonic circulation.

In February the main part of the outflow reaches the deeper depths (500 m) and propagates as a boundary current until it reaches the Ras Al Hamra Cape, where it detaches from the coast (as seen in Fig. 2) and moves northward and then turns east while flowing along the isobaths of 500 m and forms an "*S*" shape meander. On the left side of the meander a relatively weak cyclonic circulation is formed that contain less outflow water characteristics. While on its right side a more intense anti-cyclonic eddy forms that carries more outflow features. Another small portion of the outflow still continues its motion as a boundary current until it reaches the Ras Al Hadd Cape. Here it turns right (east) as in May and forms a cyclonic eddy. We found that this cyclonic circulation has a permanent existence during both months at the place where the outflow water meets the Indian Ocean inflow water (Ras Al Hadd Cape) and possibly the Cape

OSD
6, 3057–3100, 2009

effect can contribute to its formation (as mentioned by Tao, 1987; Asaro, 1998; Pause et al., 2004). Maybe during May the commencing of Monsoon wind could contribute to intensify this circulation and causes it to appears on the surface as well.

Several eddy generation mechanisms have been argued in the literatures. For example Asaro (1998) suggested that a coastal trapped boundary current may gain anticyclonic vorticity as a result of viscous stress in the boundary layer when it arrives to a cape or canyon. Asaro used this theory to explain permanent existence of anticyclone in the Arctic Ocean. He also speculated that Mediterranean eddies (meddies) can be generated by the same mechanism as the Mediterranean outflow separates from the continental slope. Bower et al. (1997) from numerous Lagrangian observations and implementation of the Asaro model explained the reproduction of meddies at the Cape St. Vincent.

Swaters (1991) presented a two-layer theoretical model and a linear stability analysis for a dense bottom plume on a sloping continental shelf and speculated that the instability is baroclinic since the mean potential energy is released by down-slope falling of the perturbed density front on the down-slope edge of density filament. The density front is strongly coupled to the upper layer through the mechanism of vortex stretching and compression. Eddies are formed in the upper layer and travel in a direction with shallower water to their right.

Prater (1992) suggested that this may be a mechanism for the formation of anticyclone but the most likely generation mechanism for the Gulf of Cadiz meddy is the instability of the buoyancy driven coastal boundary current. He compared his finding with laboratory experiments of Griffiths and Linden (1981) for a buoyant fluid from a source adjacent to a vertical boundary in a rotating tank. Griffiths and Linden showed that with a continuous release of fluid from the source, the current grew in width and depth until it became unstable to non-axisymmetric disturbances. They also presented a two-layer model for baroclinic instability with including friction dissipation due to Ekman layers and arbitrary ratio of layer depths with no horizontal shear and showed that the wavelengths and phase velocities of disturbances from laboratory experiment were

OSD

6, 3057–3100, 2009

consistent with that of their model. Finally they argued that when the current occupied only a small fraction of total depth ($h/H<0.1$, where h and H are thicknesses of the plume and ambient water layer, respectively), barotropic processes were thought to be important with the growing waves gaining energy from the horizontal shear. The coastal trapped outflow here may be subjected to horizontal shear (barotropic) instability.

Jungclaus (1999) investigated the evolution of buoyancy driven intermediate flow along an idealized continental slope using a three-dimensional numerical ocean model (POM). He showed that the intruding outflow interacts with overlaying water and vortex compression and stretching take places. The phase relation between the lower layer and upper layer perturbations reveal the baroclinic instability as the mechanism for initial destabilization. The lateral intrusions associated with the transfer of potential energy from the mean flow to the perturbation potential energy are then transformed into the perturbation kinetic energy by the adjustment process. As the perturbations grow to large amplitudes, dipoles are formed and move off shore. He also showed that the lateral intrusion of the plume into the ambient water column compresses the water above and below and thus anti-cyclonic vorticity is introduced in order to conserve potential vorticity. Finally, he emphasized that the depth ratio of the flow layers was about 0.15–0.2 (not far from 0.1), so barotropic influences could be important Griffiths and Linden (1981).

Stern (1980) showed that for a coastal gravity current with zero potential vorticity assumption, if the current width far upstream of the nose is less than a critical fraction (0.42) of the Rossby radius of deformation (based on the current depth far upstream), then the nose of the current will propagate along the coast as a bore and the form of the nose may be steady if the friction is able to dissipate sufficient kinetic energy. If the upstream current is wider than this critical value the flow may be blocked and deflected perpendicular to the coast. With implementing the Stern theory (however the outflow vorticity may not be zero) to assume outflow different behavior at the Ras Al Hamra Cape, we extracted outflow characteristics at a place some before the Cape as: $h \sim 300,\ 500\,\mathrm{m}$ (outflow depth); $g' \sim 0.01,\ 0.02\,\mathrm{ms}^{-2}$ (reduced gravity), $w \sim 10,$

OSD
6, 3057–3100, 2009

25 km (outflow width) and $f \sim 6.0 \times 10^{-5}\,s^{-1}$ (Coriolis parameter) for May and February respectively. Therefore, the corresponding Rossby radius of deformation ($\sqrt{g'h}/f$), are approximately equal to 29 and 53 km for May and February respectively, that lead to critical current widths of order of 12 km for May and 22 km for February. In comparison between these value and outflow widths, it could be concluded that during Feburary the outflow must detach from the coast and propagate normal to the coast, while during May it must continue its propagation along the coastal boundary (as seen in Figs. 13 and 14) .

3.4 The outflow T, S characteristics

Figures 15 and 16 show typical T-S profiles at some stations shown in Fig. 1, obtained from CTD measurements and model simulations during February and May. Generally, for all temperature profiles resulted from the model simulations within the model constraints, rather poor consistencies with measurements are observed especially in upper layers. In some stations (e.g. station 7 in February) measurements show fully mixed layer down to 60 m depth while the model predicted the mixed layer with only 10 m depth. In addition, the model simulations of the surface temperatures in comparison with filed observations show to be higher up to 3 °C in February and are less by 2 °C in May (except for St. 2 in the Oman Sea that differences up to 5 °C is observed that more investigation is needed).

These differences are also observed in salinity in the upper layers but are less. As a whole, these inconsistencies can be explained by the fact that in our study we did not include the surface heat and radiation fluxes that have major roles in the model capability to simulate surface temperature and mixed layer depth. In addition, the use of mean monthly surface wind with low resolution (1 degree) and not including the tide may contribute to these incompatibilities. Since we intended to study the PG outflow as a density current formed on the bottom beginning to spread in the Oman Sea (far from the surface forcing) these assumptions may have minor influences in our study.

OSD
6, 3057–3100, 2009

In these comparisons, the nearest grid points of the model to the location of measurements were selected and so in some cases inconsistency in depths are observed. It is necessary to say that some time variability in the simulation profiles, especially in the Oman Sea leads to poor agreements of the results with limited measurements. This can be due to pulsing nature of the outflow due to its interaction with tidal front at the Strait of Hormuz (Matsuyama, 1998) as well as mechanisms of instability generations in the Oman Sea (Paus et al., 2004).

The evolutions of outflow source water characteristics from Persian Gulf to the Oman Sea where it reaches the equilibrium depths are presented in Fig. 17. As the outflow passes on the bottom topography in the Strait of Hormuz, its temperature is nearly the same and is about 21 °C, but its salinity slowly decreases due to mixing with surrounding fresh waters. Once the outflow reaches the continental break in the Oman Sea its salinity decreases during both months.

During February, over a distance about of 50 km a strong decrease in the outflow salinity from 40 to 38.6 psu occurs, but its temperature changes a little. After that, the outflow sigma-T become nearly fixed (about 27 kgm^{-3}) and thus it has gained its equilibrium depth. The outflow continues to propagate with no substantial variations in its T, S characteristics at a distance of about 100 km. Then a noticeable decrease in both the outflow temperature (more than 3 °C) and its salinity (about 1 psu) occurs while its density is still constant as before. These decreases occur after the outflow is separated from the coast and bottom topography at the Ras Al Hamra and begin to meander. Here, the detachment of an anti-cyclonic eddy from the main outflow could be the reason to these decreases.

During May, the decrease in the outflow salinity occurs about 100 km earlier in comparison with February. This may be related to different mechanisms that outflow experiences during its propagation. The differences in the T, S outflow characteristics during Febuary and May lead to different outflow densities and probably causes different outflow pathways. The less outflow density and thus less stratification and warmer surrounding water during May, may lead to earlier more mixing as observed in Fig. 17.

OSD
6, 3057–3100, 2009

At this stage the outflow salinity decreases (more than 0.5 psu) while its temperature increases (about 1.5 °C). Here the outflow sigma-T is about 26.5 kgm^{-3} and stays nearly constant for a distance of about 150 km. While the outflow salinity decreases to about 37 psu, there are fluctuations in its temperature between 19 and 24 °C hence, the outflow sigma-T is also varying between 25 and 26.5 kgm^{-3}. These can be inferred from the horizontal salinity horizontal sections (Fig. 10) that during May some parts of the outflow appears as some patches of salt water in vicinity of shallow depths near the western and southern coasts. Since we plot the outflow T-S evolutions as maximum salinity at some selected cross-sections and the corresponding temperature, the fluctuation in temperature of the outflow can be related to existence of the maximum salinities at shallower depths area and also in deeper part with lower temperature and hence, higher density.

The T-S diagrams of the water masses in the Oman Sea encompassed in the box shown in Fig. 1 are presented in Fig. 18. As shown in the diagrams the outflow in the Oman Sea appears as water masses with more salinity and thus more density. During February its salinity is more than 40 psu and its temperature is nearly constant and is between 20–21 °C that leads to sigma-T values with more than 29 kgm^{-3}. In comparison, during May the outflow appears as a salty water mass with salinity less than 40 psu and temperature variations between 20–24 °C (that may be related to the existence of the outflow at different depths according to above argument) and its sigma-T occasionally reaches more than 28 kgm^{-3}. At the surface the salinity seems to be between 36–36.5 psu in both months. The surface temperatures are about 25 °C and 27 °C for February and May, respectively, and the existence of the anti-cyclonic warm center eddy (Fig. 10) with temperature more than 26 °C are clear in February diagram.

4 Conclusions

A numerical study of the PG outflow including its impacts on the physical properties of the Oman Sea has been carried out using a three-dimensional numerical model. The

OSD
6, 3057–3100, 2009

implemented model was the Princeton Ocean Model that has been used widely for estuarine, coastal waters and open-ocean application modeling. The simulations were preformed for two times of the year (mid winter and early summer) as direct CTD measurements at western boundary of the model domain as thermohaline characteristics of the Persian Gulf outflow were available, and also only mean monthly wind forcing at the surface was applied. We did not include the tidal components in our simulations by assuming that the outflow condition is during the neap tide, when its maximum discharge is expected (as pointed out by Matsuyama, 1998), and hence it is not affected much by tide.

The model simulations were appropriately verified by a few available observations and some previous works. However, some inconsistencies were observed in temperature profiles especially in the upper layers that are mainly due to neglecting surface heat fluxes in the model. In addition, in the Oman Sea some inconsistencies were observed between model salinity profiles and observations that probably are because of intermittency of the outflow as it interacts with tidal front in the Strait of Hormuz (Matsuyama, 1998) and probably the outflow instability.

Our simulations showed that the saltier and hence denser outflow source water during February relative to May leads to deeper sinking in the Gulf before it reaches the Strait of Hormuz and thus it disappears from surface well inside the Gulf. Also, the surface wind can contribute to more eastward propagation of the upper layer waters towards the Oman Sea during May.

When the outflow exits the Persian Gulf as a bottom density current it gradually turns to the right due to Coriolis effect and begins falling down on the continental slope because of its higher density while moving along the western and southern coasts. The denser outflow during Feburary causes it to penetrate more into deeper depths relative to May (mean depth of 500 m versus 300 m). Nevertheless, the outflow main pathways are nearly the same until it reaches the Ras Al Hamra Cape. During February the outflow that is flowing in the deeper parts is more affected by the steep slope topography (as seen in Fig. 2). The topography causes the outflow depth to increase (due to

OSD
6, 3057–3100, 2009

stretching processes) and so the compression of water column above and below of the outflow takes place. Therefore, as a result of conservation of the potential vorticity an anti-cyclonic circulation is introduced (as speculated by Jungclaus, 1999). Although, small portion of the outflow still is flowing along the side boundary until reaching the Ras Al Hadd Cape.

In contract to February in May, the outflow is flowing in the upper layer until it meets the Ras Al Hamra Cape, and it is less affected by the steep topography and so continues to propagate as before in vicinity of the side boundary until it reaches the Ras Al Hadd Cape. Here, an anti cyclonic circulation is observed for both months of simulation that is probably due to the interaction of the Persian Gulf outflow water with Indian Ocean waters. During May with the beginning of the south-west Monsoon, the surface inflow of Indian Ocean current is intensified and so the anti-cyclone is strengthened from surface to depths.

As a whole, we find that the seasonal variations of the outflow source water characteristics may lead to different outflow pathways due to different mechanisms that outflow experiences in the Oman Sea and Indian Ocean. The mechanisms include variety of dynamical processes such as barotropic and baroclinic instabilities as well as effects of complicated topography and geometry of the Strait of Hormuz and Oman Sea that influence the outflow spreading pathways and eddy generations in the region.

Lastly, it is necessary to say that this is a primary study to address some features of the Persian Gulf outflow. We are going to extend our modeling domain to include the entire Persian Gulf, Oman sea and Northwest Indian Ocean also considering all the surface forcing as well as river discharges and tidal components in order to better understand the effective parameters on the formation and seasonal variations of the outflow and its influences on generation of the Persian Gulf eddies (Peddies) in the Oman Sea.

OSD
6, 3057–3100, 2009

References

Bidokhti, A. A. and Ezam, M.: The structure of the Persian Gulf outflow subjected to density variations, Ocean Sci., 5, 1–12, 2009, http://www.ocean-sci.net/5/1/2009/.

Bidokhti, A. A.: Shear induced splitting of a plume outflow in a stratified enclosed basin, Indian J. Mar. Sci., 34(2), 192–211, 2005.

Blumberg, A. F. and Mellor, G. L.: A description of a three-dimensional coastal ocean circulation model, In Three-Dimensional Coastal Ocean Models, edited by: Heaps, N., American Geophysical Union, 1–16, 1987.

Brewer, P. G., Fleer, A. P, Kadar, S., Shafer, D. K., and Smith, C. L.: Report A: Chemical oceanographic data from the Persian Gulf and the Gulf of Oman, Rep. WHOI-78-37, 105 pp., 1978.

Bower, A. S., Armi, L., and Ambar, I.: Lagrangian observations of meddy formation during a Mediterranean Undercurrent seeding experiment, J. Phys. Oceanogr., 27, 2545–2575, 1997.

Bower, A. S., Hunt, H. D., and Price, J. F.: Character and dynamics of the Red Sea and Persian Gulf outflow, J. Geophys. Res., 105(C3), 6387–6414, 2000.

Elliott, A. J. and Savidge, G.: Some features of the upwelling off Oman, J. Mar. Res., 48, 319–333, 1990.

D'Asaro, E. A.: Generation of submesoscale vortices: A new mechanism, J. Geophys. Res., 93, 6685–6693, 1988.

Chao, S. Y., Kao, T. W., and Al-Hajri, K. R.: A numerical investigation of circulation in the Persian Gulf, J. Geophys. Res., 97(C7), 11219–11236, 1992.

García Berdeal, I., Hickey, B. M., and Kawase, M.: Influence of wind stress and ambient flow on a high discharge river plume, J. Geophys. Res., 107(C9), 3130, doi:10.1029/2001JC000932, 2002.

Fer, I. and Ådlandsvik, B.: Descent and mixing of the overflow plume from Storfjord in Svalbard: an idealized numerical model study, Ocean Sci., 4, 115–132, 2008, http://www.ocean-sci.net/4/115/2008/.

Geernaert, G. L., Katsaros, K. B., and Richter, K.: Variation of the drag coefficient and its dependence on sea state, J. Geophys. Res., 91, 7667–7679, 1986.

Griffiths, R. W. and Linden, P. F.: The stability of vortices in a rotating stratified fluid, J. Fluid Mech., 105, 283–316, 1981.

Griffiths, R. W. and Linden, P. F.: The stability of buoyancy-driven coastal currents, Dyn. Atmos. Oceans, 5, 281–306, 1981.
Johns, W. E., Yao, F., Olson, D. B., Josey, S. A., Grist, J. P., and Smeed, D. A.: Observations of seasonal exchange through the Strait of Hormuz and the inferred heat and freshwater budgets of the Persian Gulf, J. Geophys. Res., 108(C12), 3391, doi:10.1029/2003JC001188, 2003.
Jungclaus, J. H.: A three dimensional simulation of the formation of anticyclonic lenses (meddies) by the instability of an intermediate depth boundary current, J. Phys. Oceanogr., 29, 1579–1598, 1999.
Jungclaus, J. H. and Mellor, G. L.: A three-dimensional model study of the Mediterranean outflow, J. Mar. Syst., 24, 41–66, 2000.
Kantha, L. H., Blumberg, A. F., and Mellor, G. L.: Computing phase speeds at an open boundary, J. Hydraul. Eng., 116, 592–597, 1990.
Kantha, L. H. and Clayson, C. A.: Numerical models of oceans and oceanic processes, International Geophysics Series, Volume 66, Academic Press, 940, 2000.
Matsuyama, M., Kitade, Y., and Senjyu, T.: Vertical Structure of current and density front in the Strait of Hormuz, Offshore Environments of the ROPME after the War related Oil-Spill, 23–34, 1998.
Mellor, G. and Yamada, T.: Development of a Turbulence Closure Model for Geophysical Fluid Problems, Rev. Geophy. Space Phys., 20(4), 851–875, 1982.
Mellor, G. L.: Users guide for a three-dimensional, primitive equation, numerical ocean model, P. Atmos. Ocean. Sci., Princeton University, 2003.
Mesinger, F. and Arakawa, A.: Numerical methods used in atmospheric models, GARP Publication Series, No. 14, WMO/ICSU Joint Organizing Committee, 64 pp., 1976.
Orlonski, I.: A simple boundary condition for unbounded hyperbolic flows, J. Comput. Phys., 21, 251–269, 1976.
Pous, S. P., Carton, X., and Lazure, P.: Hydrology and circulation in the Strait of Hormuz and the Gulf of Oman result from the GOGP99 Experiment, J. Geophys. Res., 109, C12037, doi:10.1029/2003JC002145, 2004.
Prater, M. D.: Observations and hypothesized generation of a meddy in the Gulf of Cadiz. Ph.D. thesis, University of Washington, 143 pp., 1992.
Reynolds, R. M.: Overview of physical oceanographic measurements taken during the Mt. Mitchell Cruise to the ROPME Sea Area, Mar. Pollut. Bull., 27, 35–59, 1993.

OSD
6, 3057–3100, 2009

Senjyu, T., Ishimaru, T., Matsuyama, M., and Koike, Y.: High salinity lens from the Strait of Hormuz, Offshore Environments of the ROPME after the War related Oil-Spill, 35–48, 1998.
Serra, N., Ambar, I., and Kase, R. H.: Observations and numerical modeling of the Mediterranean outflow splitting and eddy generation, Deep Sea Res., 52, 383–408, 2005.
Stern, M. E.: Geostrophic fronts, bores, breaking and blocking waves, J. Fluid Mech., 99, 687–704, 1980.
Swaters, G. E.: On the baroclinic instability of cold-core coupled density fronts on a sloping continental shelf, J. Fluid Mech., 224, 361–382, 1991.
Swift, S. A. and Bower, A. S.: Formation and circulation of dense water in the Persian Gulf, J. Geophys. Res., 108(C1), 3004, doi:10.1029/2002JC001360, 2003.

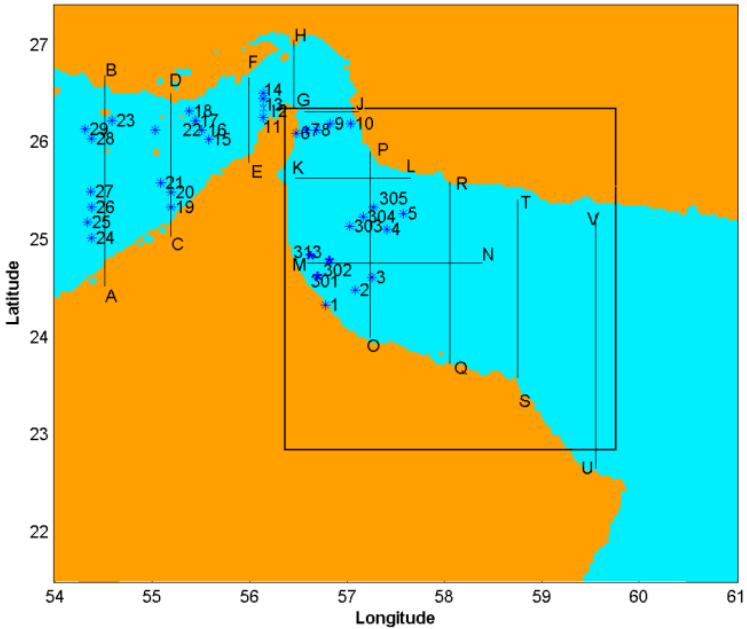

Fig. 1. Location of CTD stations during ROPME expedition (1992). The lines exhibit the paths of cross-sections that the model results are extracted.

OSD

6, 3057–3100, 2009

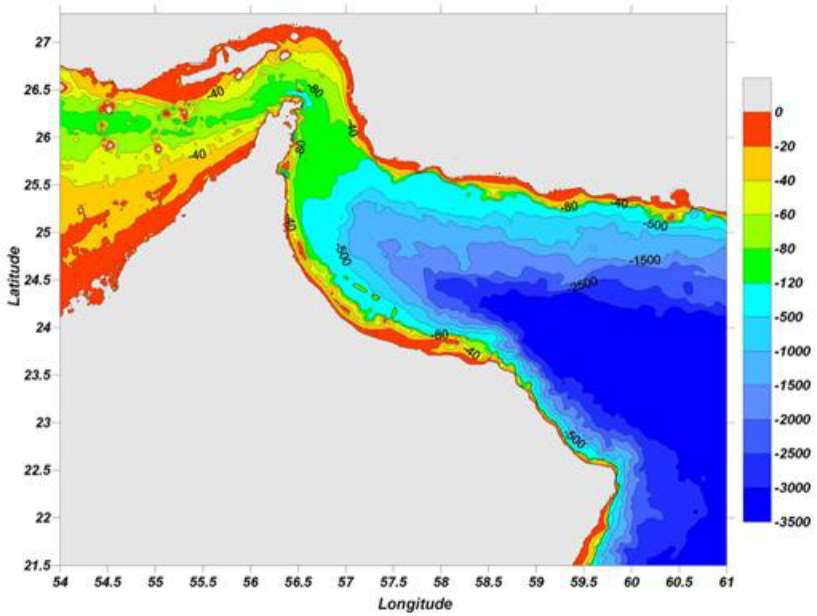

Fig. 2. Model domain and topography including east of Persian Gulf, Oman Sea and north-west of Indian Ocean.

OSD
6, 3057–3100, 2009

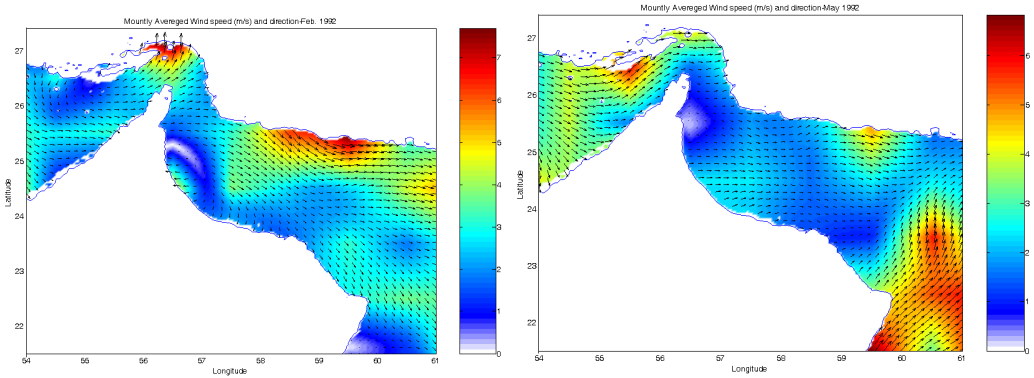

Fig. 3. Mean monthly wind patterns on the model domain in February (left) and May (right) 1992.

OSD
6, 3057–3100, 2009

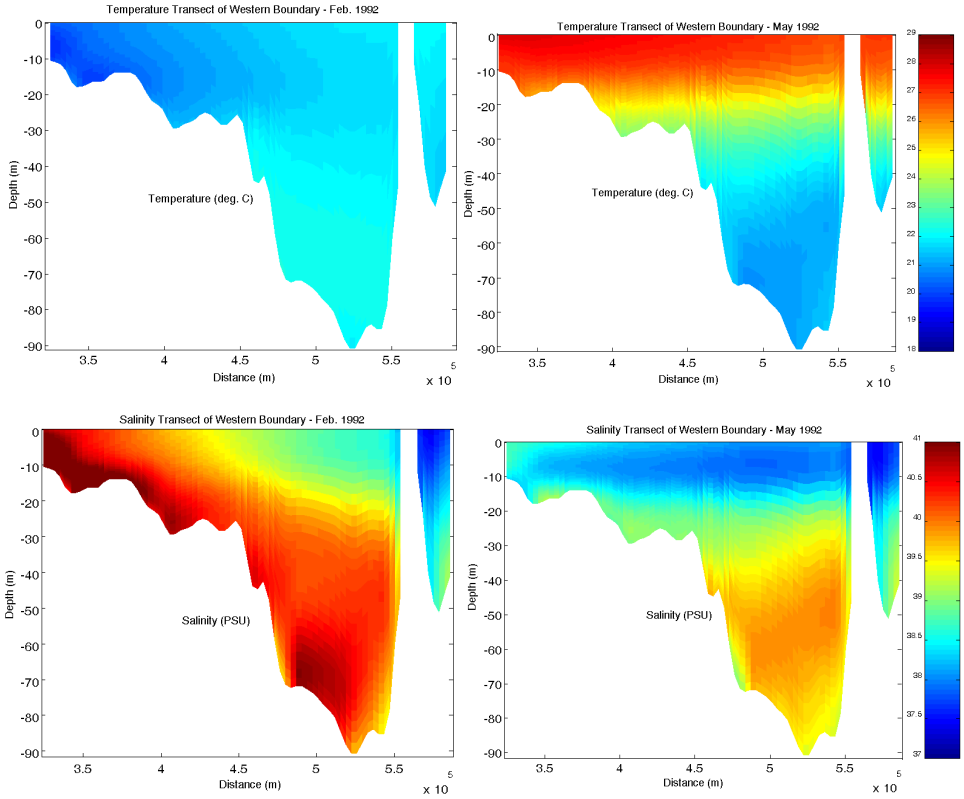

Fig. 4. Temperature and salinity transects for February and May 1992 on the western boundary of model domain after processing the CTD data.

OSD

6, 3057–3100, 2009

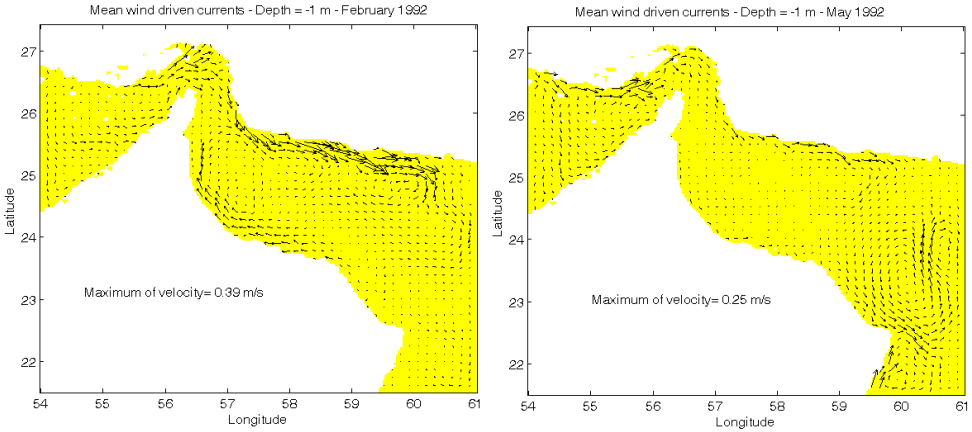

Fig. 5. Mean wind driven currents during February (left) and May (right).

OSD
6, 3057–3100, 2009

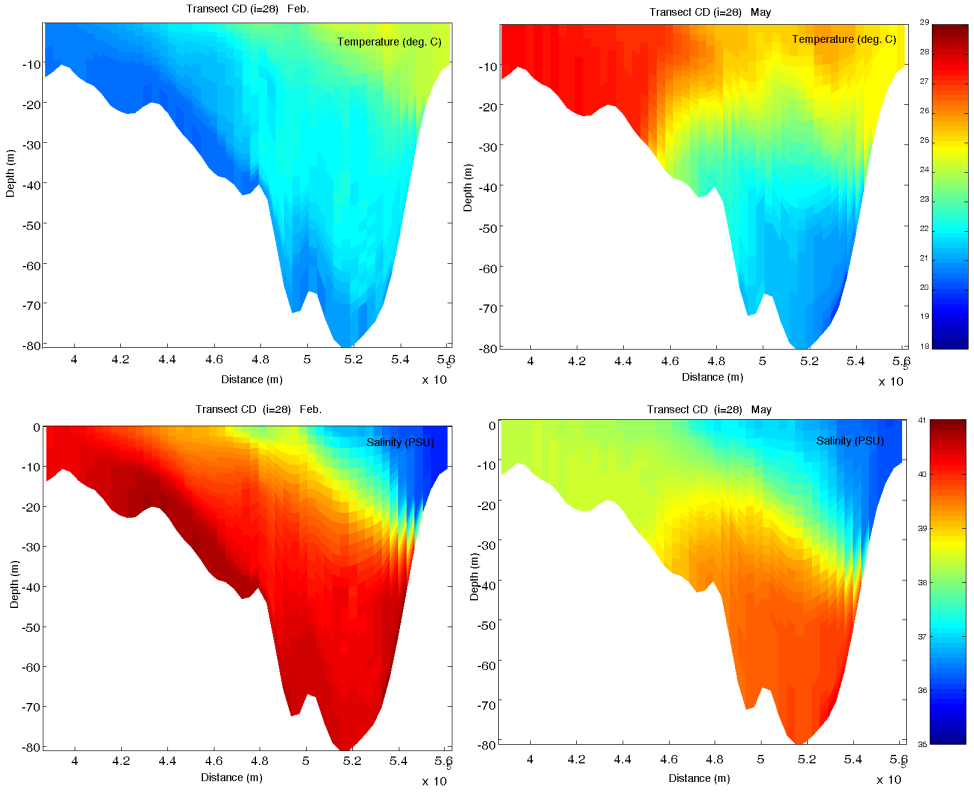

Fig. 6. Cross-section of temperature and salinity along CD path, shown in Fig. 1 obtained from model simulation during February (left) and May (right).

OSD

6, 3057–3100, 2009

Numerical simulations of spreading of the Persian Gulf outflow

M. Ezam et al.

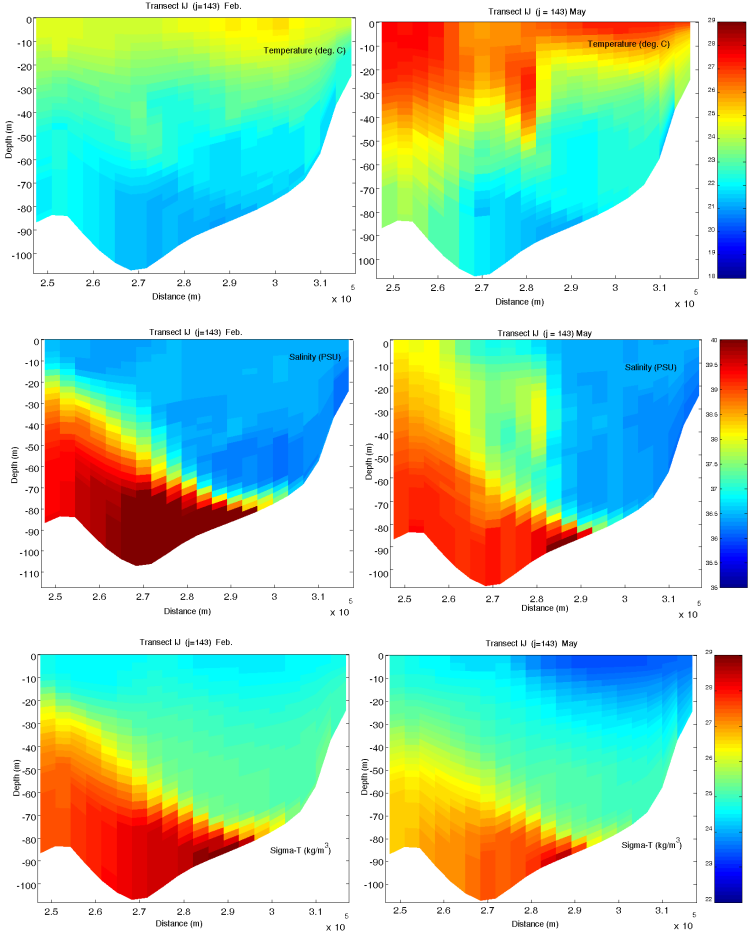

Fig. 7. Cross-section of temperature, salinity and sigma-*T* along IJ path, shown in Fig. 1 obtained from model simulation during February (left) and May (right).

OSD
6, 3057–3100, 2009

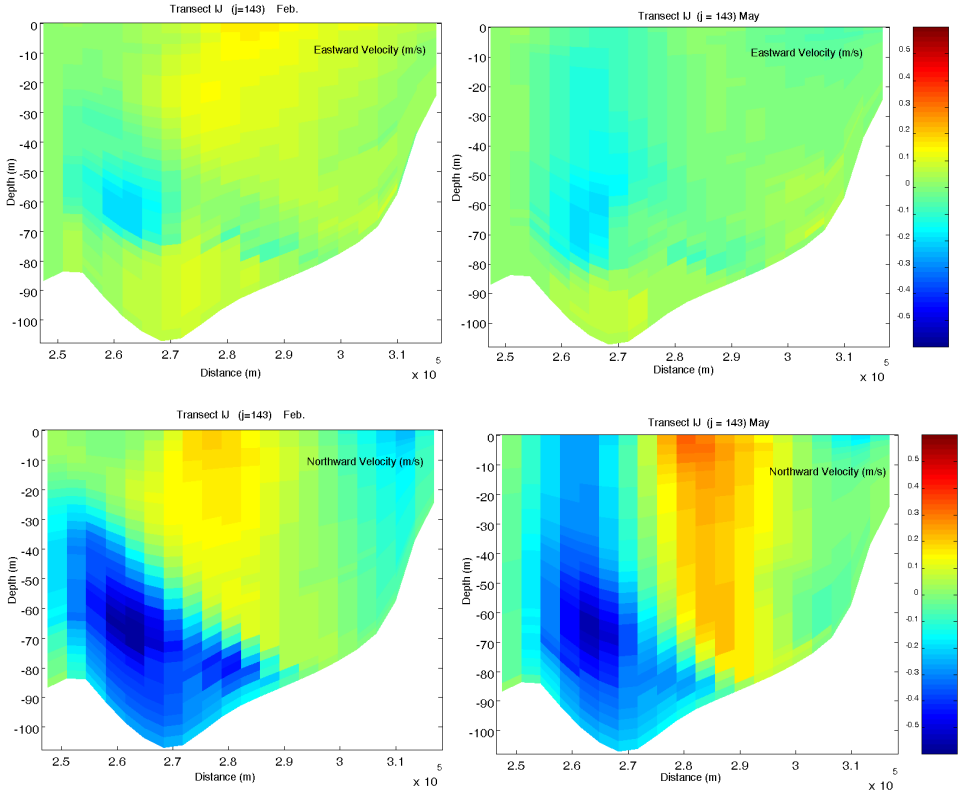

Fig. 8. Cross-section of velocity components along IJ path shown in Fig. 1, obtained from model simulation during February (left) and May (right).

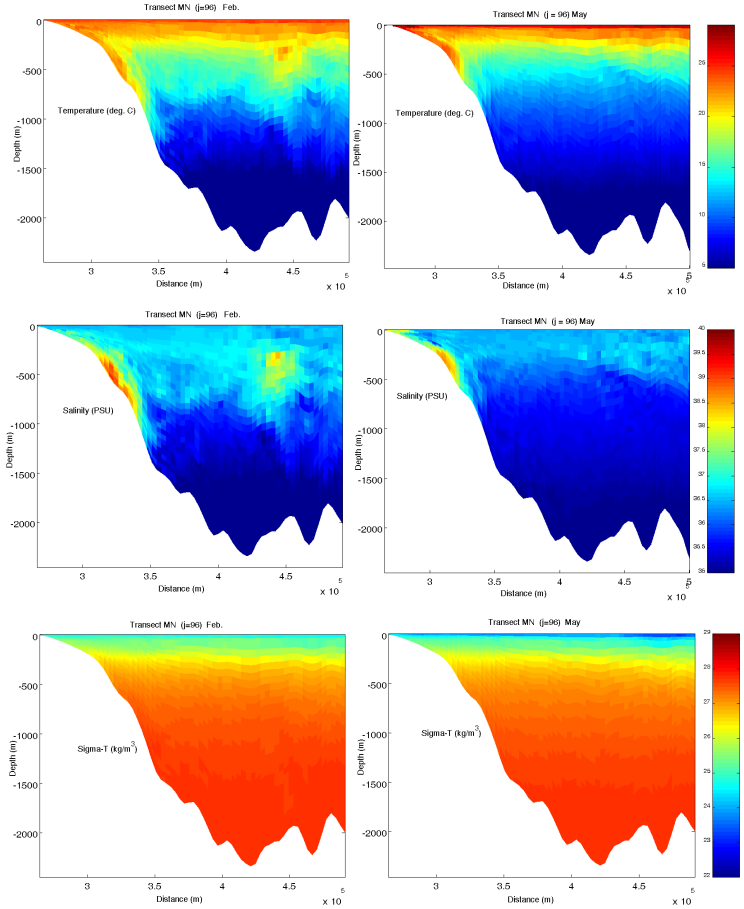

Fig. 9. Cross-section of temperature, salinity and sigma-*T* along MN path, shown in Fig. 1 obtained from model simulation during February (left) and May (right).

OSD

6, 3057–3100, 2009

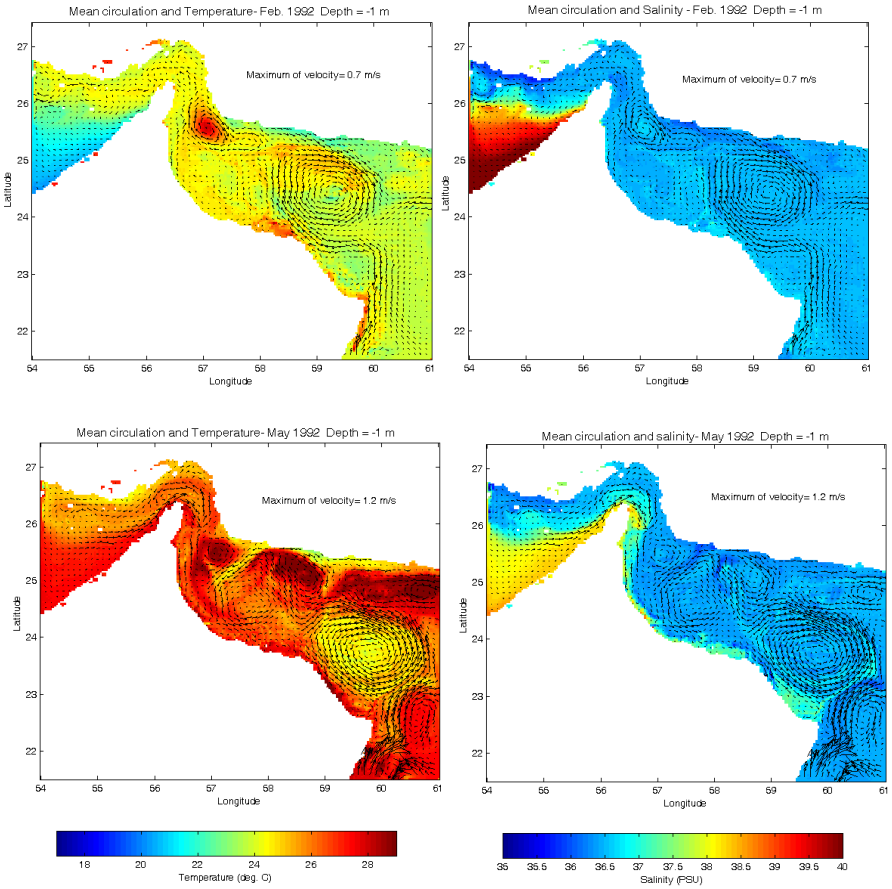

Fig. 10. Horizontal temperature and salinity fields at depth 1m for February (up) and May (down).

OSD
6, 3057–3100, 2009

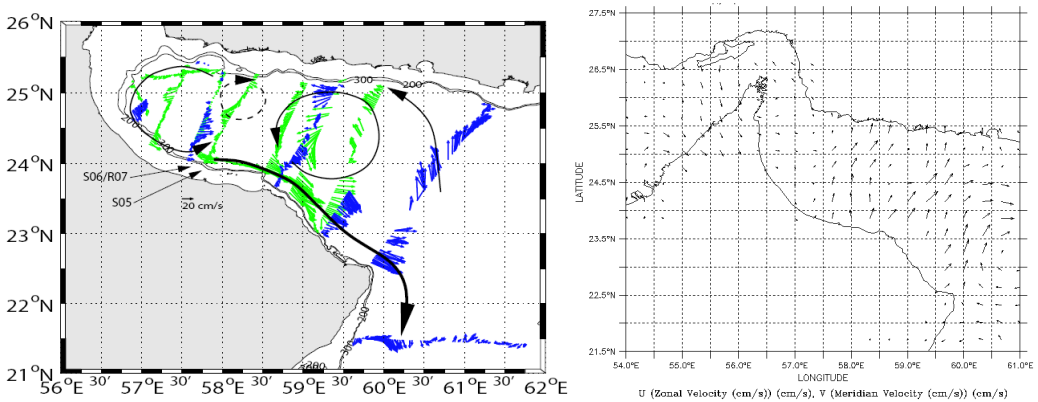

Fig. 11. Circulation pattern in the Oman Sea: sketched from field measurements at upper 300 m during October and early November 1992 (Pous et al., 2004) (left). Geostrophic velocities at 17 February 1993 from NOAA/PMEL (right).

OSD
6, 3057–3100, 2009

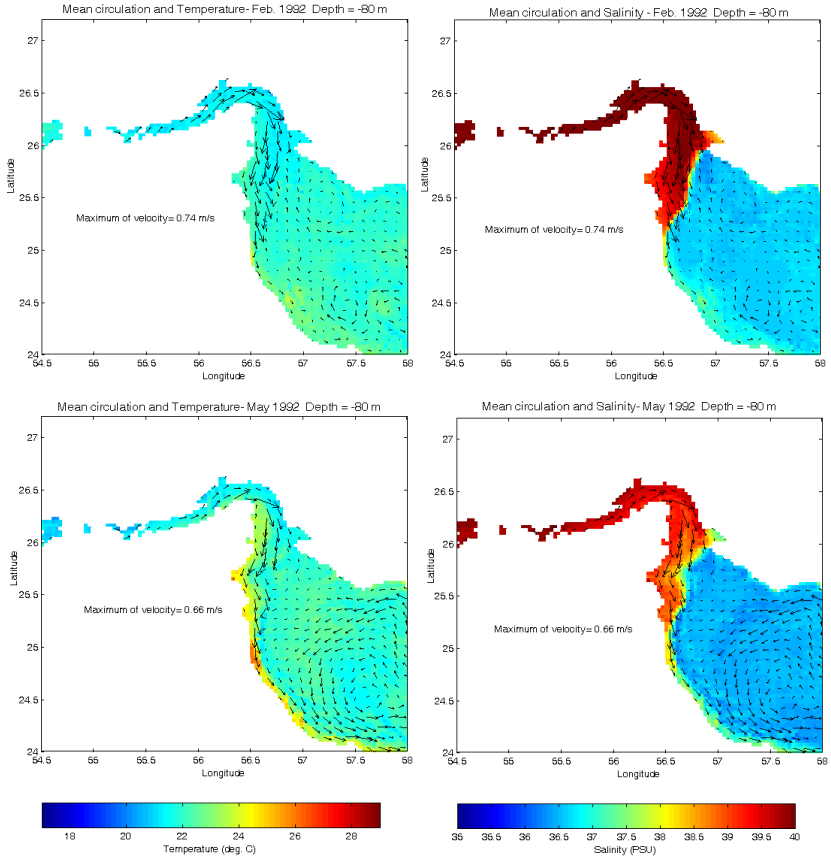

Fig. 12. Horizontal temperature and salinity fields in extended view of Strait of Hormuz at depth 80 m.

OSD
6, 3057–3100, 2009

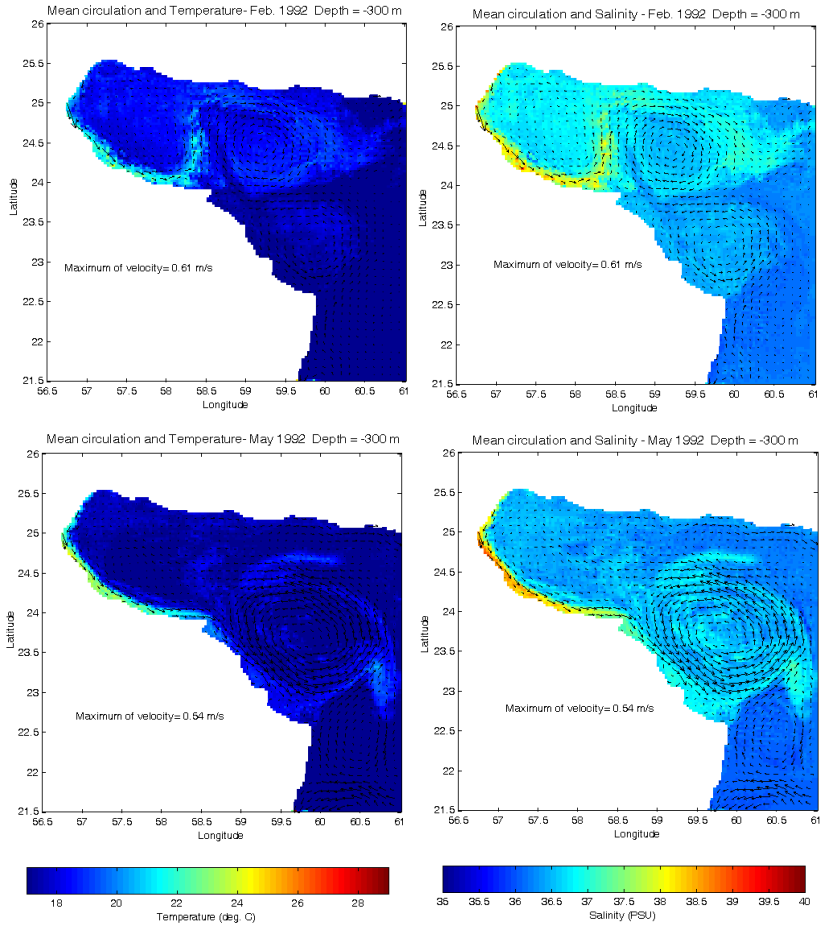

Fig. 13. Horizontal temperature and salinity fields at depth 300 m for February (left) and May (right), obtained from model simulations.

OSD
6, 3057–3100, 2009

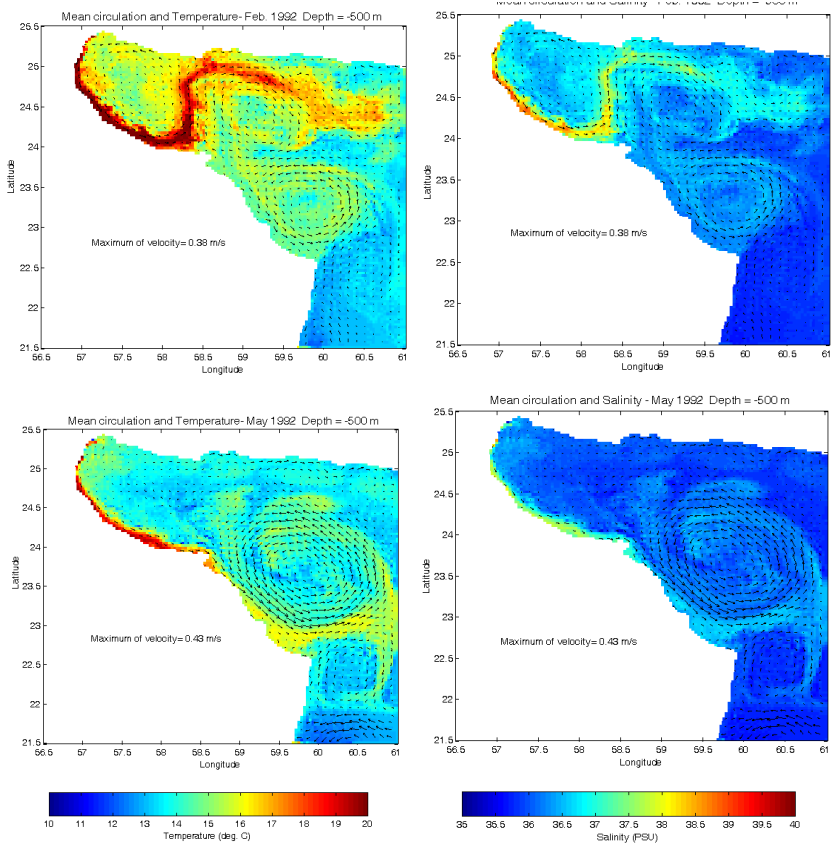

Fig. 14. Horizontal temperature and salinity fields at depth 500 m for February (left) and May (right), obtained from model simulations.

OSD

6, 3057–3100, 2009

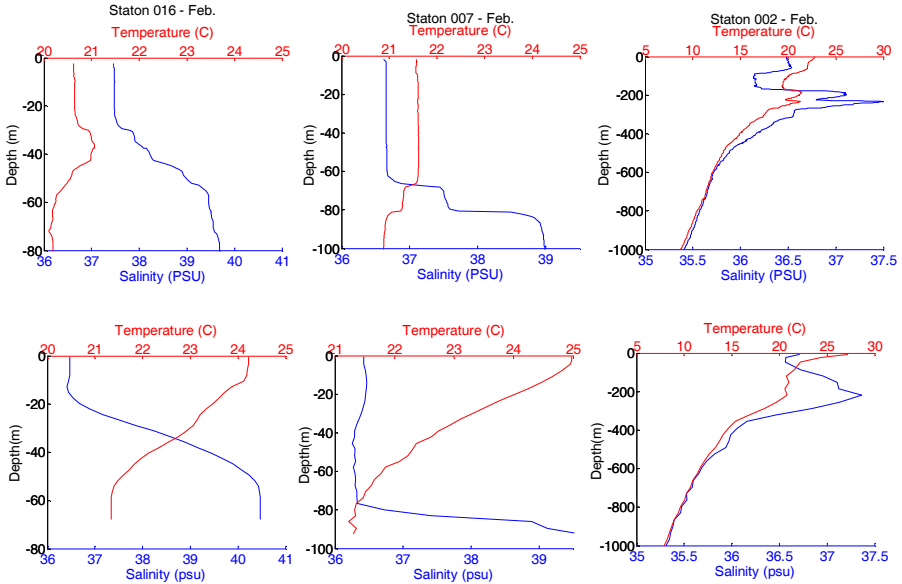

Fig. 15. Typical salinity- temperature profiles during February from CTD measurments (up) and model simualtions (down). Locations are shown in Fig. 2.

OSD
6, 3057–3100, 2009

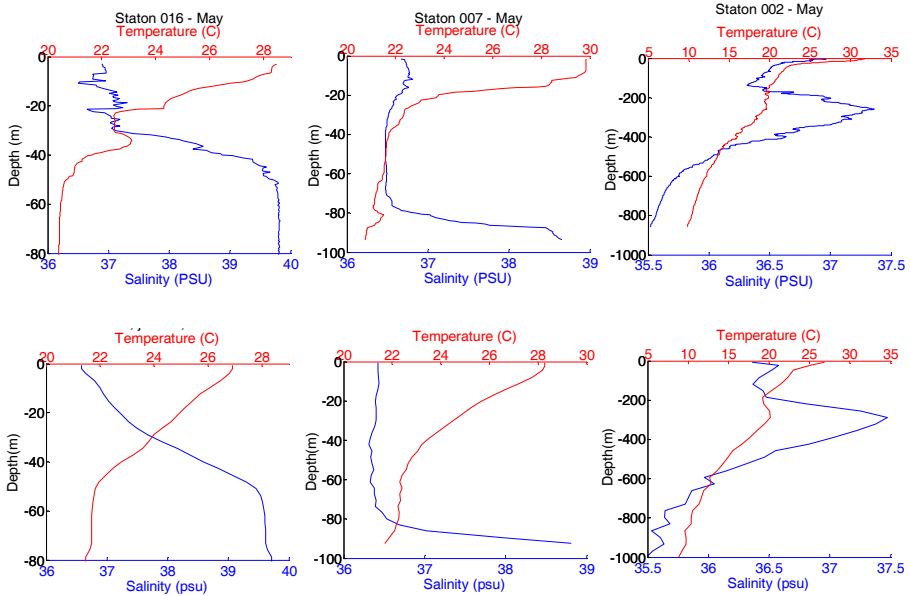

Fig. 16. Typical salinity- temperature profiles during May from CTD measurments (up) and model simualtions (down). Locations are shown in Fig. 2.

OSD
6, 3057–3100, 2009

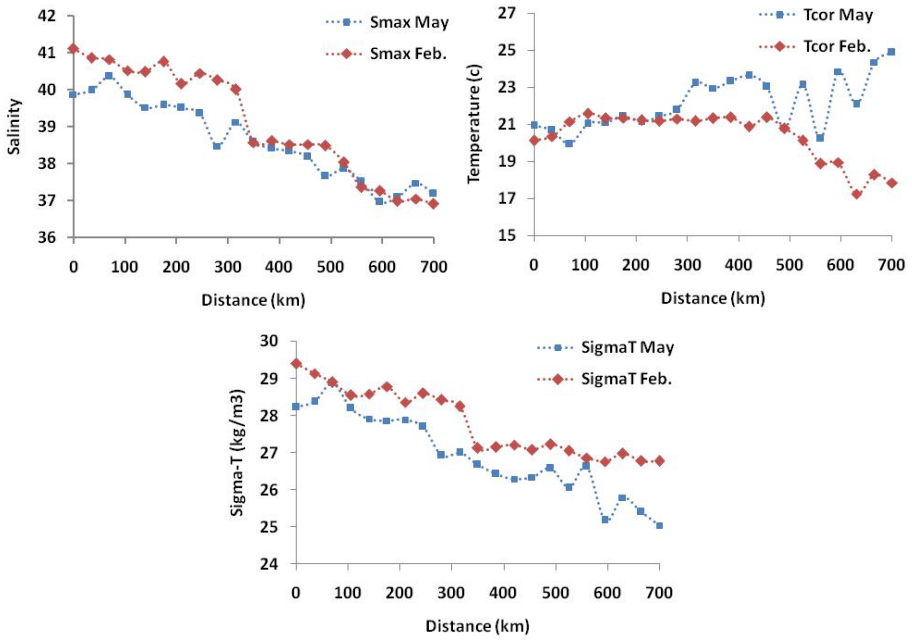

Fig. 17. Evolutions of outflow salinity, temperature and sigma-*T* from source water in the Persian Gulf to product water in the Oman Sea.

OSD
6, 3057–3100, 2009

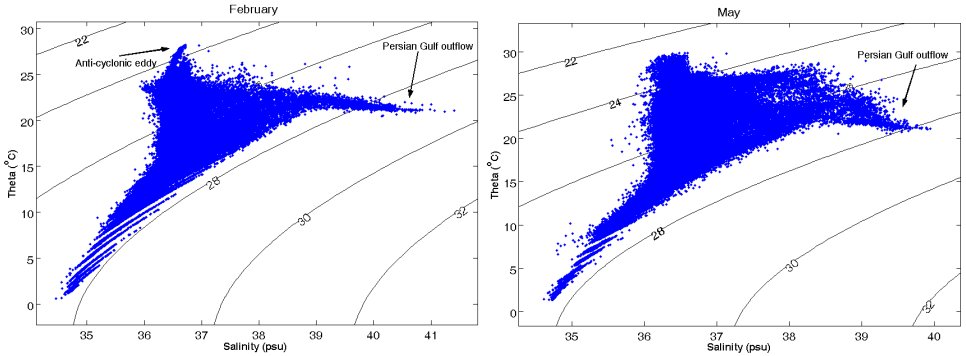

Fig. 18. *T*-*S* diagrams of water in the Oman Sea surrounded in box shown in Fig. 1 for February (left) and May (right).

OSD
6, 3057–3100, 2009